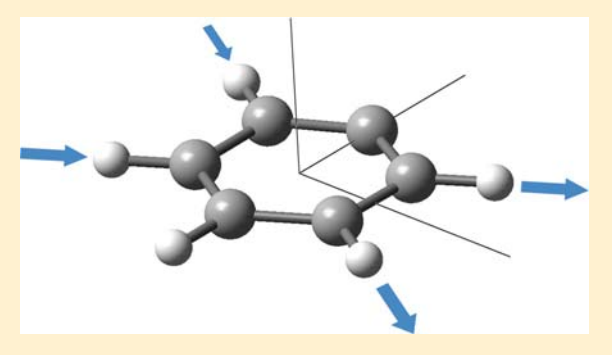


High-Resolution Rovibrational Spectroscopy of Jet-Cooled Phenyl Radical: The ν_{19} Out-of-Phase Symmetric CH Stretch

Grant T. Buckingham, Chih-Hsuan Chang, and David J. Nesbitt*

JILA, National Institute of Standards and Technology and Department of Chemistry and Biochemistry, University of Colorado, Boulder, Colorado 80309, United States

ABSTRACT: Phenyl radical has been studied via sub-Doppler infrared spectroscopy in a slit supersonic discharge expansion source, with assignments for the highest frequency b2 out-of-phase C–H symmetric stretch vibration (ν_{19}) unambiguously confirmed by ≤ 6 MHz $(0.0002~{\rm cm}^{-1})$ agreement with microwave ground state combination differences of McMahon et al. [Astrophys. J. 2003, 590, L61-64]. Least squares analysis of over 100 resolved rovibrational peaks in the sub-Doppler spectrum to a Watson Hamiltonian yields precision excited-state rotational constants and a vibrational band origin ($\nu_0 = 3071.8915(4) \text{ cm}^{-1}$) consistent with a surprisingly small red-shift (0.9 cm⁻¹) with respect to Ar matrix isolation studies of Ellison and co-workers [J. Am. Chem. Soc. 2001, 123, 1977].



Nuclear spin weights and inertial defects confirm the vibrationally averaged planarity and ²A₁ rovibronic symmetry of phenyl radical, with analysis of the rotational constants consistent with a modest $C_{2\nu}$ distortion of the carbon backbone frame due to partial sp rehybridization of the σ C radical-center. Most importantly, despite the number of atoms (N = 11) and vibrational modes (3N - 6 = 27), phenyl radical exhibits a remarkably clean jet cooled high-resolution IR spectrum that shows no evidence of intramolecular vibrational relaxation (IVR) phenomena such as local or nonlocal perturbations due to strongly coupled nearby dark states. This provides strong support for the feasibility of high-resolution infrared spectroscopy in other aromatic hydrocarbon radical systems.

I. INTRODUCTION

Phenyl radical (C₆H₅, Figure 1) is the product of homolytic CH bond cleavage in benzene and is arguably one of the most

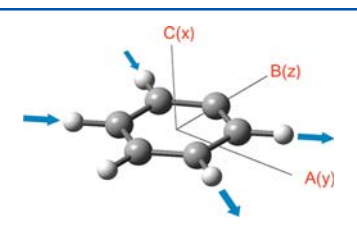


Figure 1. Phenyl radical with its body fixed principle rotation axes labeled. For $C_{2\nu}$ point group symmetry analysis, the x, y, and z axes are taken as a right-hand coordinate system pointing along the C, A, B principle axes, respectively. The arrows indicate the displacement vectors for the b_2 symmetry out-of-phase symmetric CH stretch (ν_{19}) reported herein.

fundamental aromatic hydrocarbon radical species in all of chemistry. By virtue of its aromatic character and unpaired electron, phenyl constitutes a highly reactive radical species known to play an important role in chemistry ranging from geologic formation of hydrocarbon fuels to industrial synthesis. 1,2 Of particular interest, this radical is also strongly implicated as a crucial chemical intermediate in soot formation, combustion, and polycyclic aromatic hydrocarbon (PAH)

chemistry in the interstellar medium (ISM).3-11 In multiple areas of chemistry, reaction schemes detailing the production and depletion of ring hydrocarbon species often invoke phenyl radical as a proposed intermediate, 11-14 which continues to provide strong motivation for detailed first principles understanding of its fundamental properties.

In contrast to its widespread chemical impact and importance, there is a remarkable lack of detailed spectroscopic information on phenyl radical, in particular high-resolution infrared spectroscopy in the gas phase. Indeed, a deeper understanding of the structural properties, reaction kinetics, and dynamics of radicals in general can be obtained via highresolution infrared spectroscopy of highly reactive intermediates, both in ground and vibrationally excited states. In particular, such experiments offer benchmark tests under ideal laboratory conditions with which to confirm high-level theoretical predications, as well as provide insight into complicated reaction pathways under more challenging and exotic chemical conditions. One of the reasons for this is clearly high chemical reactivity, which makes it a challenge to prepare

Special Issue: Oka Festschrift: Celebrating 45 Years of Astrochemistry

Received: January 21, 2013 March 27, 2013 Revised: Published: March 28, 2013

phenyl radical in sufficiently high densities per quantum state to allow such detailed characterization to be feasible. This is particularly true for relatively large polyatomic radical species with small rotational constants such as phenyl radical, for which rotational partition functions under conventional temperature conditions can be quite large and thus yielding correspondingly low populations per quantum state.

In combustion chemistry, phenyl radical is a proposed intermediate in both synthetic and destructive pathways of PAH systems.³ The importance of phenyl radical is especially relevant for heavy oil and tar sand deposits, which greatly exceed the existing reserves of conventional oil, but require additional chemical processing due to their significant PAH content.¹⁵ In order to convert such reserves into cleaner and more efficient fuel sources, the hydrogen-to-carbon ratio can be increased by catalytic hydrocracking, which uses homolytic bond cleavage of large aromatic molecules to yield lower molecular weight combustible reagents.¹⁶ Indeed, for conjugated hydrocarbon systems such as those present in heavy fuel sources, phenyl radical is directly produced through breaking the biaryl C-C bonds, a process known as hydrogenolysis.¹⁷ In addition, mechanisms for combustion of even simple aliphatic fuels also highlight phenyl radical as a critical species in the net production of aromatics and therefore a key intermediate on the path to the formation of macroscopic soot.18

Although much less well determined at present, phenyl radical is thought to play an equally central role in astrochemistry. In particular, it has been definitively established that PAHs are indeed present in the ISM19,20 with phenyl radical a likely key player in the underlying chemistry. For example, reaction schemes such as those presented by Wang and Frenklach³ highlight phenyl radical as a critical reactive intermediate in the conversion from the simplest aromatics (e.g., benzene) to larger PAH species. This so-called hydrogenabstraction-C₂H₂-addition (HACA) is initiated by activation of benzene via removal of a hydrogen atom to yield phenyl radical, which then reacts with acetylene to form H + phenylacetylene. Subsequent hydrogen abstraction from the α -carbon followed by a second C₂H₂ addition produces a diacetylenic radical. This species can rapidly undergo electron rearrangement to produce a bicyclic aromatic radical, which in turn may either proceed with further C₂H₂ additions or terminate via hydrogen atom addition to yield naphthalene. Indeed, such HACA pathways have been adapted from combustion chemistry and applied to PAH formation in carbon rich stars^{3,20-23} where the high temperatures (~1000 K) can provide sufficient energy to overcome the significant activation barriers for such a reaction

Interestingly, such combustion motivated HACA mechanisms are challenging to invoke in explaining the formation of PAHs in the ISM, where the much lower temperatures (≈ 10 K) would strongly limit such activated processes. Of particular relevance, therefore, crossed molecular beam experiments by Tielens et al. have recently discovered a barrierless reaction between phenyl radical and vinylacetylene, whereby naphthalene can be produced in a single collision event, even at low temperatures similar to those found in the ISM. Clearly, definitive confirmation of such mechanisms for PAH synthesis in astrochemical environments will require considerable additional work, for which observational spectroscopy of relevant reaction intermediates such as phenyl radical may offer critical support. Indeed, phenyl radical is indicated as an

intermediate for both low and high temperature reaction pathways, for which advanced knowledge about phenyl radical is needed to facilitate accurate predictions of its concentration and chemical activity. By way of example, the precursor molecule benzene has recently been observed spectroscopically in the proto-planetary nebula CRL 618.²⁵ Infrared, millimeter, and/or microwave detection of phenyl radical spectra in collocated regions of space could provide critical supporting evidence for such reaction mechanisms as well as information on kinetics of PAH formation.²⁶ This, in turn, could significantly advance future prospects for successful search for these species in the ISM with new far-IR/submm telescope capabilities coming on line.^{27–29} Such detection and confirmation efforts would greatly profit from accurate spectroscopic characterization by laboratory studies of gas phase phenyl radical, toward which the present work is directed.

The infrared C-H stretch region of phenyl radical has been studied previously in the condensed phase via matrix isolation spectroscopy,³⁰ but of the 5 normal mode stretches predicted in the infrared CH stretch energy region, there has been remarkably little success at obtaining further information by high-resolution gas phase efforts.³¹ Indeed, there are only two sources of high-resolution spectroscopic data on phenyl radical to date: (i) pioneering microwave studies by McMahon et al,³² and (ii) a recent communication from our group³¹ on highresolution infrared studies of phenyl in a slit jet discharge. We have since then considerably improved our experimental conditions for phenyl radical production, and recently exploited this experimental capability for high-resolution spectral search throughout the 3000-3200 cm⁻¹ near-infrared region. Such efforts have yielded detailed gas phase spectra for 3 of the 5 fundamental CH stretch spectral bands in this near-IR region. The focus of this work is a more complete description and analysis of the b_2 out-of-phase symmetric CH stretch mode, ν_{19} , with spectral results for two weaker a₁ symmetry CH stretching modes (ν_1 and ν_2) modes currently under analysis and to be presented elsewhere.

What is particularly noteworthy about this observation is that, despite the relatively large number of atoms in phenyl radical, the CH stretch spectra can be clearly rovibrationally resolved, unambiguously assigned, and successfully analyzed. This is far from an obvious result, since large polyatomic hydrocarbon molecules with correspondingly many vibrational modes can exhibit extensive coupling between excited zero order vibrational "bright states" and the dense bath of near resonant "dark states" that are energetically accessible at C-H stretch frequencies. 33-36 The lack of strong rovibrational state coupling evident in the high-resolution phenyl radical spectra indicates surprisingly small complications due to intramolecular vibrational relaxation (IVR) of energy, which bodes promisingly for high-resolution spectroscopy of other cyclic aromatic radical species, as well as potentially even more complicated PAH radical systems.

The outline of this paper is as follows. The experimental setup is described briefly in section II, including a description of the pulsed slit jet discharge and present methods of producing frequency stabilized tunable IR light. Section III presents results and analysis of the spectroscopic data, with discussion of the relevant experimental findings in section IV. In particular, the rotational constants and nuclear spin statistics offer insight into the structural planarity, in-plane distortion, and rovibronic symmetry of the molecule, while the simplicity of the gas phase rovibrational spectrum at the fundamental vibrational level

indicates a remarkable lack of unimolecular dynamics due to intramolecular vibrational coupling effects. Section V summarizes the main results and conclusions.

II. EXPERIMENTAL SECTION

The ability to obtain well-resolved rovibrational spectra of phenyl radical in the gas phase relies largely on several experimental advantages: (i) high radical densities per quantum state accessible with low temperature discharge expansions, (ii) sub-Doppler compression of velocity broadening in the slit jet, (iii) long absorption path geometry, and (iv) precisely tunable frequency stabilized IR light source. The experimental setup has been described in previous papers, thus only a brief summary of details relevant to the present work need be presented here.

The spectroscopic target phenyl radical species is produced via CX bond fragmentation of monohalobenzenes (C_6H_5X) in a slit supersonic jet expansion, yielding typical signal-to-noise on the strongest absorption peaks of roughly 50:1. The mechanism for CX bond fission is presumably electron dissociative attachment to form the radical center + X-, which would clearly favor use of halogenated precursor species with weakest CX bond strengths. Indeed, phenyl radical can be efficiently synthesized in the discharge with bromobenzene and iodobenzene, but with signal intensities greatly limited by reduced vapor pressures at room temperature. As a compromise between vapor pressure, control and formation efficiency, the carrier gas Ne70 (70% neon, 30% helium) is therefore bubbled through liquid-phase chlorobenzene cooled at 0 °C, with the gas mixture further diluted with Ne70 to produce 0.5% C₆H₅Cl gas samples in the stagnation region at 280 Torr total pressure. The gas is supersonically expanded through a JILA-built solenoid-driven slit valve capable of generating intense pulses with tunable duration (1000 μ s, < 50 μ s rise time) that exit through a 4 cm long, 300 μ m wide slit into a vacuum chamber. This supersonic expansion is triggered at a repetition rate of 19 Hz, with pressure in the vacuum chamber maintained <50 mTorr by a 560 L/second Roots blower (Leybold WS200). During each gas pulse, a 50 kHz modulated square wave voltage ($\approx 500 \text{ V}$) is applied across an insulated 1 mm region located immediately prior to the expansion orifice, as illustrated in Figure 2. This voltage is sufficient to produce a glow discharge with 280 mA peak current through the sample and carrier gas mixture, which causes dissociative electron attachment and homolytic cleavage of the CCl bond to produce the desired phenyl radical.

The slit jet expansion rapidly cools the phenyl radical down to $\approx 11(1)$ K, where infrared light 5 mm downstream from the nozzle orifice permits for direct absorption by the newly formed radical molecules. Near shot noise limited absorption sensitivities on the order of 0.002% ($A = 2 \times 10^{-5}$) in a 10 kHz bandwidth are made possible by fast servo loop subtraction of signal and reference detector technical common mode noise on the IR laser. The signal is further augmented by increasing the absorption path length using of a 16-pass Herriott cell, which is aligned directly below the slit orifice. This alignment minimizes molecular velocity parallel to the beam path, lowers the Doppler width of the measured absorption peaks by an additional 5-10 fold (in Ne70), and thereby increases the peak absorption cross section by an equivalent 5-10 fold. In combination with the much slower $(1/r \text{ vs } 1/r^2)$ density drop off in a slit versus pinhole jet, this yields a net sensitivity enhancement for direct IR absorption on high reactive radicals

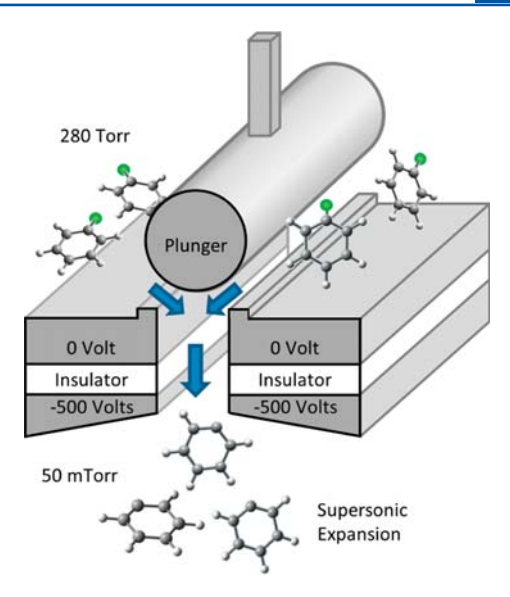


Figure 2. Cartoon diagram of pulsed slit jet discharge. During the $1000~\mu s$ gas pulse, the carrier gas and precursor flow into the discharge region where a square wave modulated voltage (-500~V) is applied with a 50~kHz frequency. The electric field induced glow discharge results in efficient electron dissociative attachment of the weak carbon—halogen bond. This high concentration of phenyl radicals is then rapidly cooled to $\approx 11(1)~K$ in the slit supersonic expansion.

by some 3-4 orders of magnitude. Combined with typical integrated absorption strengths (5-20 km/mol)³⁹ for hydrocarbon species such as phenyl radical, these absorption sensitivities translates into minimum detectable number densities of $(2-8) \times 10^8 \text{ #/cm}^3/\text{quantum state in a detection}$ region 5 mm downstream of the slit jet orifice. Indeed, based on calculated integrated absorption cross sections for the present ν_{19} out-of-phase symmetric CH stretch band, infrared light is produced by spatially overlapping two visible laser beams in a temperature controlled, periodically poled lithium niobate crystal, which results in difference frequency generation of tunable light in the $2.5-4 \mu m$ region. The two visible light sources are (i) a fixed frequency argon ion (Ar⁺) laser operating at 514 nm (19429.88 cm⁻¹) and (ii) a tunable ring dye laser (R6G dye) between 17500 to 16000 cm⁻¹. The Ar⁺ laser is locked via servo-loop to the transmission fringes of an external Fabry-Perot cavity (FSR = 250 MHz), which in turn is locked to a polarization-stabilized helium-neon (HeNe) laser to achieve a long-term frequency stability over multiple days. Scanning progress of the dye laser is measured with respect to fringes on the same ultrastable Fabry-Perot cavity, yielding comparable precision for frequency measurement on the difference frequency IR light. Absolute frequencies are determined by reference absorption line of jet cooled methane $(R(4),\ 3067.3000\ cm^{-1})$ observed under identical slit jet conditions,⁴⁰ providing a calibrated IR frequency axis with typical root-mean-square (rms) reproducibility of 8 MHz (<0.0003 cm⁻¹) for the transitions reported.

The IR light is divided into two beams by a 50:50 beam splitter, with one portion measured directly on a liquid nitrogen cooled InSb reference detector. The remainder of the IR light is then directed through the slit jet discharge/Herriott cell vacuum chamber, extracted after 16 passes, and recollimated onto a matched liquid nitrogen cooled InSb signal detector. Noise between signal and reference detector is actively

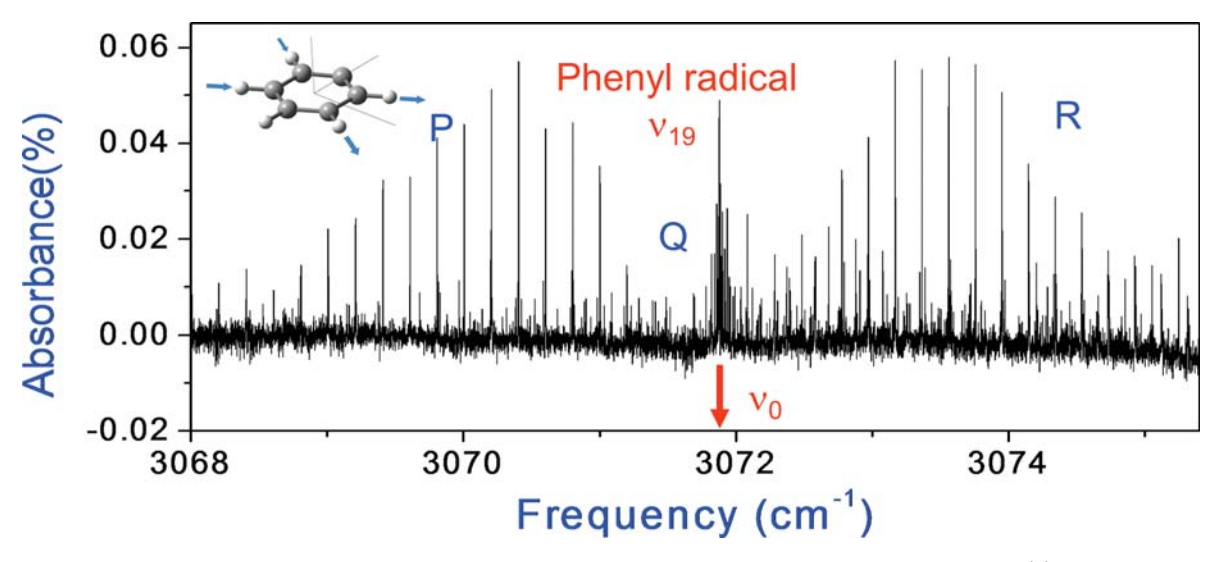


Figure 3. Overview rovibrational spectrum of the symmetric out-of-phase C–H stretch, ν_{19} , in phenyl radical at $T_{\rm rot} \approx 11(1)$ K. The band origin is at 3071.8915 cm⁻¹, with extensive P, Q, and R branch structure clearly evident. In spite of spectral overlap due to the near oblate top nature of phenyl radical, the combination of supersonic jet cooling and sub-Doppler transverse velocity compression allows for assignment and analysis of over 100 fully resolved rovibrational transitions.

balanced using high bandwidth (1 MHz) home-built active subtraction electronics, with the weak absorption signals at the 50 kHz discharge modulation frequency obtained via lock-in detection to provide additional signal-to-noise enhancement. These lock-in detection signals are then further analyzed in the time domain by gated integration and differential baseline correction before, during and after the slit jet pulse, with all resulting data and frequency diagnostics stored in a computer for later analysis.

III. RESULTS AND ANALYSIS

Phenyl radical is predicted to be a planar, near-oblate asymmetric top with a rigid structure described by $C_{2\nu}$ point group symmetry with x, y, and z axes pointing along the C, A, and B principle axis directions (see Figure 1). Normal mode analysis predicts five infrared active fundamental modes in the 3000-3200 cm⁻¹ region consisting of predominantly CH stretching character. There are three CH stretch vibrations of a₁ symmetry, which, in order of decreasing frequency, can be predominantly characterized as (i) in-phase, symmetric stretch of all 5 CH bonds (a_1 , ν_1 , 3192 cm⁻¹), (ii) out-of-phase, symmetric stretch between the ortho (i.e., carbon atoms 2,6) and para (i.e., carbon atom 4) CH bond positions (a_1 , ν_2 , 3180 cm⁻¹), and (iii) in-phase, antisymmetric stretch of the corresponding ortho/meta CH bonds (a₁, ν_3 , 3160 cm⁻¹). In addition, there are 2 CH stretch vibrations of b₂ symmetry: (i) out-of-phase, symmetric stretch (b_2 , ν_{19} , 3182 cm⁻¹) and (ii) out-of-phase, antisymmetric stretch (b₂, ν_{20} , 3166 cm⁻¹) of the ortho/meta CH bonds. The predicted frequencies for these five vibrations are based on anharmonic scaling (0.9637(31)) B3LYP/6-31++g(3pd,3df) predictions of Dong et al., 38,39 which in turn have been benchmarked against a comprehensive set of high-resolution CH stretch spectra for hydrocarbon radicals. Of the five IR active CH stretching modes, the b₂ symmetric out-of-phase CH stretch (ν_{19}) is predicted from simple density functional calculations [B3LYP/6-311++g-(3df,3pd)] to have the largest integrated infrared intensity (S_0 ≈ 17.3 km/mol).³⁹ A sample overview spectral region for the phenyl radical in the slit jet discharge absorption spectrometer is shown in Figure 3, revealing extensive rotationally resolved P, R branch progressions and a clear Q branch feature near 3071.9 cm⁻¹. Typical isolated line absorbances are $\approx 0.04\%$, which for the above integrated absorption cross section translates into a typical number density per quantum state of $\approx 3 \times 10^9$ radicals/cm³ in the slit jet probe region and $\approx 5 \times 10^{10}$ radicals/cm³ extrapolated up toward the discharge slit orifice. Although this represents a > 10-fold lower formation efficiency than observed for other hydrocarbon radicals in the slit jet discharge geometry, this nevertheless translates into a respectable S/N ≈ 20 for typical absorbance sensitivities of 0.002% in our detection bandwidth.

As discussed in detail below, this rotational structure is indeed predominantly due to the symmetric out-of-phase CH stretch (ν_{19}) band, with a dipole derivative moment along the A principal axis and thus an A-type band dominated by $\Delta K_a = 0$ and $\Delta K_c = \pm 1$ transitions. Closer inspection also reveals additional B-type band transitions from the much weaker a₁ totally symmetric ν_1 CH stretch vibration fortuitously occurring in the same spectral region, which is not considered herein. The ν_{19} Q-branch feature band origin near 3071.9 cm⁻¹ is in quite good agreement with and indeed suggests an unusually small red shift with respect to Ar matrix isolation studies ($\nu_{19} = 3072$ cm⁻¹) performed by Ellison and co-workers.³⁰ The highresolution capabilities of the slit jet expansion are often sufficient for resolving spin-rotation fine structure and sometimes even nuclear spin-electron spin hyperfine structure in these open shell systems. In the case of phenyl radical, however, these fine structure contributions are known from microwave studies to be quite small ($\varepsilon_{\rm cc} \approx 4.8~{\rm MHz}$) and in fact are seen only as unresolved additional broadening beyond the sub-Doppler limit.³² To be consistent with our other studies, however, we will nevertheless refer to total angular momentum simply by the end-over-end rotational quantum number N, although at even higher resolution these levels would of be split into doublets by coupling with electron spin (S = 1/2).

Due to H atom loss and ring distortion of the C radical center, the degeneracy of the in-plane principle rotation axes is broken (A \geq B > C), which makes phenyl radical a near-oblate

Table 1. Ab Initio Theoretical and Experimental Rovibrational Constants^a

	theory b (CCSD(T)/vtz-f12)			experiment		
	benzene	"sp² phenyl"	phenyl	benzene (gnd state)	phenyl (gnd state)	phenyl (u_{19})
$A \text{ (cm}^{-1})$	0.19024	0.20472 (+7.6%)	0.20980 (+10.2%)	0.189751(25)	0.209472(10) (+10.3%)	0.209380(4) (+10.3%)
$B (cm^{-1})$	0.19024	0.19024 (0.0%)	0.18720 (-1.6%)	0.189751(25)	0.186793(7) (-1.6%)	0.186578(4) (-1.7%)
$C (cm^{-1})$	0.09512	0.09861 (+3.6%)	0.09893 (+4.0%)	0.094876(13)	0.098714988(2) (+4.0%)	0.0986098(8) (+4.0%)
Δ	0	0	0		0.046	0.089

"High level ab initio predictions⁴⁸ (left three columns), obtained at a fixed CCSD(T)/vtz-f12 level to facilitate quantitative comparison, reflect (i) benzene, (ii) "sp² phenyl" (i.e., equilibrium benzene geometry with one hydrogen removed), and (iii) phenyl radical. The three rightmost columns represent experimentally determined values for (i) benzene, 47,69 (ii) ground state phenyl radical, and (iii) ν_{19} phenyl radical excited in the out-of-phase symmetric CH stretching mode. To aid quantitative comparison, fractional changes in each quantity with respect to theoretical and experimental values for benzene are indicated in %. b Ab initio MOLPRO calculations. 48

asymmetric top. Though the total angular momentum N remains a conserved quantum number, the unsigned body fixed projections of N along the A and C principle axes, K_a and K_c offer a further useful designation of energy levels by N_{KaKc} . Though these projection quantum numbers are only approximate for an asymmetric top, the even (e) or odd (o) nature of K_a and K_c is rigorous, since these correspond to ± 1 eigenvalues for body fixed $C_2(y)$ and $C_2(x)$ rotation operators that commute with the total Hamiltonian. As a result, the rotational energy levels of phenyl radical can be readily solved by expanding the total asymmetric top Hamiltonian in a Wang basis set comprised of symmetric/antisymmetric linear combinations of oblate symmetric top functions (e.g., 1/ $\sqrt{2\{|NK\rangle \pm |N-K\rangle}$ for K = even/odd, where K is the signed projection along the C axis. Rotational constants for phenyl radical are then obtained by iterative assignment of absorption peak frequencies to rovibrational transitions $(N'_{Ka'Kc'} \leftarrow N''_{Ka''Kc''})$ in a least-squares fitting program based on a Watson asymmetric top Hamiltonian. Due to the low rotational temperatures ($\approx 11(1)$ K) in the jet expansion, these fits are sufficient to reproduce the transition frequencies to within experimental precision without need for higher order centrifugal distortion terms, and thus the choice of reduction and representation is arbitrary.

For a near oblate asymmetric top, the eigenenergies for a given N decrease with increasing K_c , which implies most favorable Boltzmann factors for low K_a values with $K_c \approx N$. Furthermore, for a *planar* near-oblate top (i.e., $A \approx B \approx 2C$), the structure of each K_c subband is shifted by $\approx 2(X - \overline{B})K_c \approx$ $-\overline{B}K_{o}$, which for alternate K_{c} values approximately matches the $\approx 2\overline{B}$ spacing in the P and R branch progressions. The net result is a closely spaced progression of transitions with a natural propensity for spectral overlap. We therefore begin the assignment using only spectrally fully resolved and isolated features in the P and R branch region. The advantage of this approach is that it permits immediate confirmation from twoline combination differences based upon microwave spectroscopy of Thaddeus et al.,³² to which the present assignments match within 6 MHz (0.0002 cm⁻¹). Therefore, the ground state constants are held fixed at the microwave values, with the excited vibrational state rotational constants (A', B', and C')and vibrational band origin ν_0 subject to refinement in this first round of least-squares fit.

This initial P/R branch analysis provides a sufficiently good fit to the Watson Hamiltonian to enable confident spectral prediction of fully resolved albeit weaker spectral structure within the central Q branch. With the inclusion of these additional Q branch lines in the fit, the spectral predictions are now sufficiently accurate to confidently identify the weaker

individual P and R branch lines ($N \neq K_c$ and/or $\Delta N \neq \Delta K_c$) that do not satisfy requirements for both high Boltzmann population and Hönl–London factor line strength. This iterative process results in more than 100 spectrally isolated transitions that can be unambiguously assigned and least-squares fit to extract high resolution rotational constants (see Table 1) and a band origin. Even without centrifugal distortion terms, the random errors in such a least-squares analysis yield a residual standard deviation of 0.00037 cm $^{-1}$ (11 MHz), i.e., roughly comparable to rms experimental error in our frequency measurements.

At closer inspection, a small Q branch region for ν_{19} phenyl radical is expanded in Figure 4, with the band origin designated

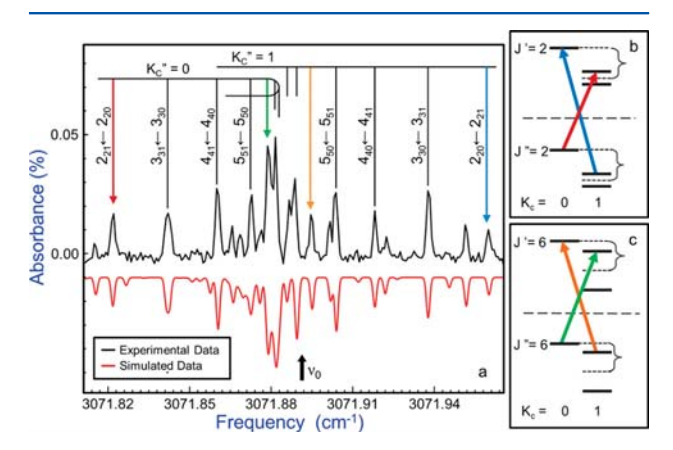


Figure 4. (a) Q branch region of the phenyl radical out-of-phase CH symmetric stretch, band origin (3071.8915 cm $^{-1}$) labeled with a black arrow. The simulated spectrum using experimental fits is shown below in red. (b,c) Rovibrational energy level diagrams highlighting the N=2 ← 2 and 6 ← 6 Q-branch manifold transitions. Color coded arrows in panel a correspond to transitions in panels b and c.

with a black arrow. The predicted spectrum (downward, red line) is generated using experimental least-squares fit constants and recapitulates the high-resolution experimental spectrum (upward, black line) of phenyl radical quite well. As seen in Figure 4, due to compensating Hönl-London factors, the strongest peaks in the Q-branch occur near the band origin and correspond to transitions that originate from higher energy states with $K_a'' \approx N''$ and $K_c'' \approx$ small, with corresponding Q-branch transitions out of the lower energy states (i.e., with $K_a'' \approx$ small and $K_c'' \approx N''$) shifted significantly to higher ($\Delta K_c = -1$) and lower ($\Delta K_c = +1$) transition frequencies from ν_0 . If we focus on the Q branch transitions with small frequency shifts, these form clear blue ($\Delta K_c = +1$) and red ($\Delta K_c = -1$) shaded

progressions out of $K_c'' = 0$ and $K''_c = 1$, respectively, converging upon one another near the band origin. This behavior can be rationalized by the right-hand panels in Figure 4, which illustrate the approximate energy level dependence on N, K_a , and K_c for pairs of Q-branch transitions. For low Nvalues, the energy difference between $K_c = 0$ and the mean of the split $K_c = 1$ levels is approximately independent of N (i.e., $\Delta E \approx (C - B)K_c^2$, while the $K_c = 1$ asymmetry splitting for low $N (\Delta E \approx 1/2 (A - B)N(N + 1))$ grows quadratically with N. With increasing N, therefore, the $N'_{N'1} \leftarrow N''_{N''0}$ and $N'_{N'0} \leftarrow$ $N''_{N''1}$ progressions necessarily shift to the blue and red, respectively. For sufficiently high N, however, the asymmetric top energy level pattern approaches a more prolate top behavior, with the $N_{\rm N0}$ and $N_{\rm N1}$ states converging to form pairs of K_c asymmetry split levels for $K_a = N$. The net result is that the $N'_{N'1} \leftarrow N''_{N''0}$ and $N'_{N'0} \leftarrow N''_{N''1}$ Q-branch progressions converge to the same transition frequency. Indeed, for negligible changes in upper and lower state rotational constants, this would predict a perfect convergence of transitions at the band origin, as is the qualitative trend evident in Figure 4. With a reliable spectral assignment in hand, we can similarly look at a sample data region in the P and R branches (see Figure 5). As

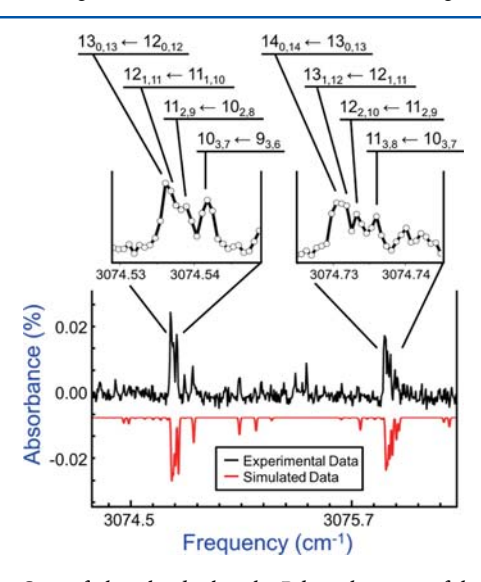


Figure 5. Scan of phenyl radical in the R branch region of the ν_{19} CH stretch. The simulated spectrum based on experimentally fit rotational and vibrational constants is shown below in red. The spectral congestion observed in these rotational structures arises naturally for a perpendicular band in a planar, near-oblate asymmetric top ($A \approx B \approx 2C$), for which the P/R branch spacings are near commensurate with sub-band spacings as a function of K_c .

expected for a near oblate planar asymmetric top ($A \approx B \approx 2C$), the spectral structure is dominated by nearly overlapping progressions in $\Delta N = \Delta K_{\rm c} = \pm 1$, where the congestion arises from the near commensurate match between P/R branch spacing and the shift in alternate $K_{\rm c}$ sub-band origins for an A-type band ($\Delta K_{\rm c} = \pm 1$). Nevertheless, agreement between experimental data and the partially overlapping asymmetric top predictions is clearly extremely good.

IV. DISCUSSION

A. Nuclear Spin Weights. As a first point of discussion, relative intensities in the rotationally resolved rovibrational spectrum can be used to provide additional confirmation on the

underlying nuclear spin statistics and thus rovibronic symmetry of the phenyl radical ground state. Although the most complete treatment of nuclear spin statistics in "floppy" molecules is provided by molecular permutation group theory, this is not essential in phenyl radical, for which results are readily obtained simply by assuming a rigid structure with $C_{2\nu}$ point group symmetry. 41 From a point group perspective, phenyl radical has two sets of equivalent hydrogen nuclei, each of which undergo feasible exchange by low barrier rotation of the molecule around the C_2 axis. The four hydrogen atoms (I = 1/2) have either spin up or spin down, which translates into $2^4 = 16$ total spin states for the molecule. This forms a reducible representation of the $C_{2\nu}$ point group, which can be reduced with the $C_{2\nu}$ character table to yield $\Gamma_{nuc\text{-spin}} = 10A_1 \oplus 6B_2$. To obtain nuclear spin weights, we note that Fermi-Dirac statistics requires the total wave function (Ψ_{tot}) to be antisymmetric with respect to exchange of equivalent hydrogen atoms and thus two equivalent pairs of fermions must transform symmetrically with respect to C_2 rotation. Furthermore, the eigenvalues for C_2 rotation around the B axis are +1 and -1 for asymmetric top eigenfunctions with $K_a + K_c$ = even and odd, respectively. In conjunction with a totally symmetric A₁ ground vibronic state, this corresponds to a 10:6 ratio of nuclear spin statistical weights for $K_a + K_c = \text{even/odd}$ states, respectively.

Spectroscopic confirmation of the correct nuclear spin weighting can be found in Figure 6, which shows a small segment of the Q branch for the ν_{19} stretch of phenyl radical. The top panel (in blue) shows stick plot predictions calculated with the correct nuclear spin ratio of 10:6 for $K_{\rm a}+K_{\rm c}=$ even:odd. Conversely, the stick plot in the bottom panel (in red) is the same prediction but with nuclear spin statistics

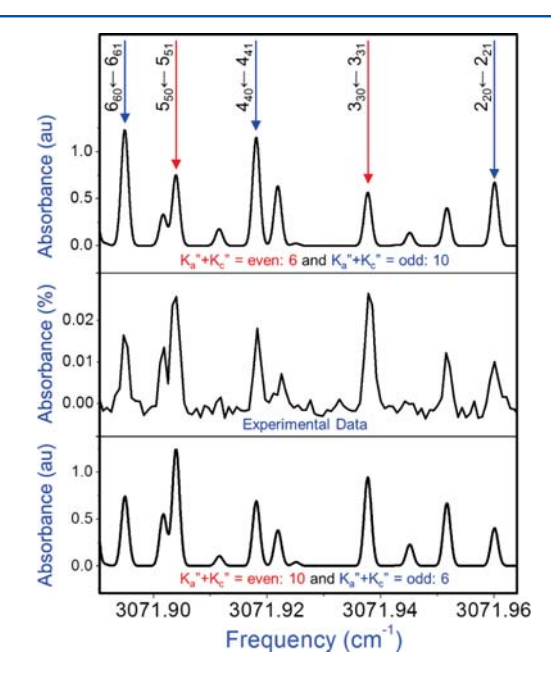


Figure 6. Comparison of two simulated spectra which highlight the effect of nuclear spin statistics in the spectrum of phenyl radical in the ν_{19} region. The middle panel shows experimental absorption spectra, whereas the lower and upper panels present intensity predictions for correct (10:6) vs inverted (6:10) nuclear spin statistical weights anticipated for $K_{\rm a}+K_{\rm c}={\rm even/odd}$ levels in the ground state. These nuclear spin weights confirm the $^2{\rm A}_1$ electronic symmetry of the ground state and thus the σ nature of the C radical center.

reversed, i.e., 6:10 for $K_a + K_c$ = even:odd. Comparison of the two simulated stick plots with the high resolution results clearly confirms a 10:6 ratio for $K_a + K_c$ = even:odd to correctly reproduce the spectral data. It is worth noting that overall wave function symmetry with respect to rotation around the B axis is directly influenced by and therefore reports on the electronic symmetry of the ground state. Specifically, for a putative π radical ground state with B₁ electronic symmetry, C₂ rotation around the B principal axis would invoke an additional sign change, and thus the nuclear spin weights would shift from 10:6 to 6:10 for $K_a + K_c = \text{even/odd}$ states. In conjunction with the above discussion of electronic symmetry, these 10:6 nuclear spin weights can be taken as independent spectral confirmation of a ground state A₁ rather than B₁ electronic symmetry, which in turn requires a σ vs π electronic structure for the radical center on the C atom. This is also consistent with aromatic stabilization of phenyl radical, which significantly lowers the energy of the π electron cloud and makes homolytic bond cleavage to form the σ radical center the energetically preferred pathway.

B. Planarity and In-Plane Ring Distortion. The rovibrationally analyzed spectra also provide additional information on the vibrationally averaged planarity of phenyl radical, as well as evidence for a static in-plane distortion of the six-membered ring. Specifically we consider the inertial defect (Δ) , i.e., $\Delta = I_c$ $-I_a - I_b$, where I_i is obtained from a sum over all masses times the distance squared from the corresponding principle rotation axis. For a perfectly rigid, classical molecule with all mass constrained to a plane, the inertial defect should vanish identically, although systematic shifts in Δ arise due to higher order quantum effects such as finite electron mass, zero point motion of the nuclei, as well as in-plane versus out-of-plane vibrational motion. ^{42–44} Table 1 summarizes the experimental inertial defects for phenyl radical in ground and vibrationally excited states. The ground state value for phenyl is small (Δ = +0.046 amu Å²) and in fact remarkably close to benzene in its ground vibrational state ($\Delta = +0.044$ amu Å²).^{45–47} This is consistent with a planar aromatic molecular structure for phenyl radical, with the slight positive contribution to Δ arising from in-plane vibrational zero point effects. It is worth noting that this inertial defect increases by nearly 2-fold in the ν_{19} excited state ($\Delta = +0.089$ amu Å²), which is also consistent with additional CH stretch motion in one of the in-plane vibrational degrees of freedom.

Although benzene and phenyl radical have the same number of carbon atoms and π -electrons, homolytic cleavage of a CH bond results in a less saturated radical carbon that is no longer purely sp² hybridized, now mixing in partial sp character in order to generate a σ radical. To investigate distortion of the phenyl backbone away from 6-fold symmetry, we compare both a theoretical/experimental rotational constants for a progression of C₆ ring molecules in the absence/presence of such rehybridization effects due to radical formation. As summarized in Table 1, the leftmost three columns reflect theoretical rotational constant values calculated at a high but uniform ab initio level⁴⁸ (MOLPRO, CCSD(T)/vtz-f12) for (i) benzene, (ii) a fictitious fully "sp2 phenyl" species clamped at the D_{6h} benzene geometry but one hydrogen atom removed along the B axis, and (iii) phenyl radical itself with complete relaxation of the carbon backbone allowed. Percent changes in each of these theoretical values with respect to benzene are indicated in parentheses. Similarly, the next three columns represent the experimental rotational constant values for (i)

ground state benzene, and phenyl radical in the (ii) ground state and (iii) with one quanta of excitation in the ν_{19} stretch, again with fractional changes in the quantities shown in parentheses.

In the theoretically predicted values, there is clearly a substantial increase (10.2%) in the A rotational constant between benzene and phenyl radical. However, the "sp² phenyl" limit (i.e., H atom removal with no change in nuclear coordinates of the C_6 frame) accounts for only $\approx 75\%$ of the observed difference. This indicates that H atom loss can not be the only source of increase in A and that indeed the phenyl radical ring is more compressed with respect to the A-axis. The shifts in B provide further evidence for such compression of the carbon ring. Specifically, since the H atom removed originates on the B-axis, there must be identically zero change in B between benzene and "sp2 phenyl" resulting purely from H atom removal. Experimentally, however, the B constant for phenyl radical decreases by an additional 1.6% as a result of rehybridization, providing confirmation that the two pairs of meta/ortho C atoms must be on average stretched further away from the B axis than in benzene.

In the absence of a full isotope substitution study, such changes in rotational constants are insufficient to determine the nuclear coordinates of phenyl radical. However, a simple rehybridization picture consistent with these changes is illustrated in Figure 7, with coordinates taken from theoretical

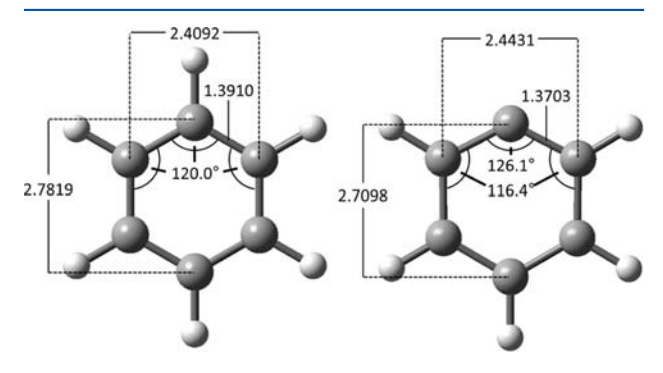


Figure 7. Ab initio theoretical comparison (CCSD(T)/vtz-f12) between benzene (left) and phenyl radical (right), illustrating the subtle distortion of the carbon ring upon H atom abstraction and radical formation.⁴⁸ The greater sp hybridization character of the unique radical carbon atom center both (i) increases the C-C-C bond angle as well as (ii) decreases the adjacent C-C bond lengths.

calculations. The unique carbon atom in phenyl radical has two filled bonding molecular orbitals with a third orbital only half occupied, thus resulting in an admixture of sp and sp² character. Partial sp character yields a greater propensity toward linear vstrigonal planar geometry that causes the C-C-C bond angle to be substantially larger ($\approx +6^{\circ}$) than the conventional 120° value for sp² bonding. Simply summarized, rehybridization of the C radical center results in (i) decreased distance of the unique carbon atom to the A axis and (ii) increased distance of the two adjacent (para) carbon atoms from the B axis. Such inplane distortion is consistent with experimental results in Table 1, which reveal an anomalously large fractional increase in A and decrease in B from phenyl radical to benzene. Alternately stated, despite having the same number of carbon atoms and π electrons as benzene, the one-half filled bonding orbital in phenyl radical clearly has measurable effects on the ring backbone geometry of the molecule. Finally, the phenyl radical

data in Table 1 indicate very good agreement between experiment and theory (<1%). Moreover, since these predictions ignore zero point quantum averaging over the vibrational wave function, the remaining discrepancies are largely systematic, for which one can empirically compensate by scaling to the ratio of experimental/theoretical values for a related molecule such as benzene. The result of such scaling improves the rotational constant agreement between theory and experiment by an additional order of magnitude ($\approx 0.1\%$).

C. Intramolecular Vibrational Dynamics. As a final topic of discussion, we consider the role of intramolecular vibrational coupling in the phenyl spectra. In high-resolution IR spectra of sufficiently large gas phase molecules, isolated transitions which carry the oscillator strength to so-called zero order "bright states" can be broadened or split into multiplets by unimolecular vibrational coupling to a typically much denser manifold of zero order "dark states." This occurs because when two or more zero order states have similar energies, residual coupling in the Hamiltonian can mix the zero order states to form eigenstates with both fractional bright and dark state character. As a result, excitation into an optically bright state necessarily prepares a coherent superposition of eigenstates, which in turn results in a time dependent transfer of vibrational energy into nearby states, or, expressed equivalently in the time domain, IVR. The critical question of interest is therefore whether typical off-diagonal IVR coupling matrix elements (i.e., $V_{ij} = \langle \Psi_{\text{dark}} | H | \Psi_{\text{bright}} \rangle$) are sufficiently large with respect to the inverse density of vibrational states (1/ $\rho(E_{\rm vib})$) for such intramolecular coupling effects to become evident in the high-resolution spectrum. Experimentally, the ν_{19} rovibrational spectrum of phenyl radical appears completely assignable and shows no effects from IVR at sub-Doppler spectroscopic resolution ($\Delta \nu_{\text{fwhm}} \approx 50 \text{ MHz} = 0.00167 \text{ cm}^{-1}$) under Ne slit discharge expansion conditions. The relevant issue is whether the (i) vibrational state density and (ii) coupling matrix elements in phenyl radical are each sufficiently small to rationalize this behavior.

The vibrational state density of a molecule at a given excitation energy grows exceptionally rapidly with the number of vibrational degrees of freedom, and in particular, the number of low vibrational modes. $^{51-57}$ Due to the presence of 3N-6=27 vibrational normal modes, the phenyl radical might be expected to suffer substantial loss of spectral simplicity from IVR induced fragmentation of isolated eigenstates of the lower order and largely separable Hamiltonian. Note that such intramolecular vibrational dynamics does not necessarily imply any true homogeneous broadening of lines beyond the sub-Doppler line width, as could occur for the case of strong predissociative coupling with the continuum. However, clearly neither scenario is the correct description, which we would experience as partial blurring in each of the high-resolution spectral samples (Figures 3-6). Instead, based on efficient backtracking state counting algorithms by Kemper et al. and simple harmonic predictions, 55 the vibrational state density per symmetry group in phenyl radical can be readily predicted to be $\rho(E_{\rm vib}) \approx 0.15 {\rm \ states/cm^{-1}}$ at $E_{\rm vib} \sim 3000 {\rm \ cm^{-1}}$, which is clearly unusually small for a molecule with 11 atoms. The obvious reason for this is its aromatic C6 ring conformation, which constrains proliferation of low frequency bends and internal torsional modes that can dramatically increase the density of states in linear hydrocarbon systems and thus the impact of mode-mode coupling.⁵⁸ In a closed C₆ ring structure, on the other hand, the lowest frequency vibrational modes are

considerably higher than for a linear C_6 chain structure, which considerable decreases the state density at typical CH stretch frequencies.

To provide some additional quantitative context, there have been systematic high-resolution IR studies of IVR coupling dynamics for hydrocarbons such as terminal CH stretch excited substituted acetylenes. ^{36,53,59} By virtue of jet cooling and sub-Doppler resolution, these studies were able to resolve the true molecular eigenstates arising from these bright state/dark state interactions in the CH stretch manifold, which thus permitted coupling matrix elements to be extracted directly from the spectra. A typical coupling matrix element size was found to be on the order of $\langle V_{ij} \rangle \sim 0.01 \text{ cm}^{-1}$, which was consistent with an empirical threshold of state density on the order of $\rho(E_{vib}) \sim$ 10² symmetry selected states per cm⁻¹ for onset of additional spectral complexity due to IVR mixing. 49,60,61 Note that this critical threshold state density is nearly 3 orders of magnitude smaller than predicted for phenyl radical at 3000 cm⁻¹ levels of internal excitation. Thus, if one were to assume a similar range of coupling matrix elements for fundamental CH stretch excitation in aromatic ring systems, this would indeed be entirely consistent with the observed lack of IVR induced fragmentation of bright states with near resonant dark states in the current phenyl radical spectra.

As a parting comment, we briefly consider the future prospects for extending such high-resolution IR studies to even larger polyatomic aromatic hydrocarbon systems. Figure 8

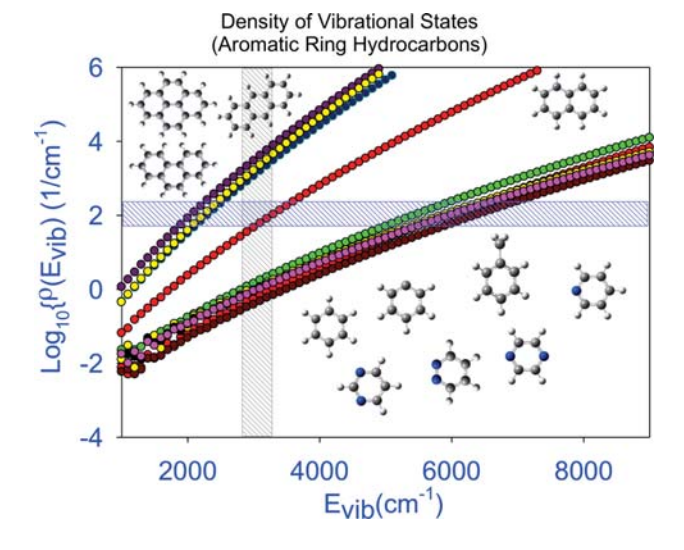


Figure 8. Estimates of symmetry selected vibrational state density (i.e., scaled to point group order) for a series of aromatic and PAH molecules, based on simple density functional predictions (B3LYP/6-311++g(3df,3pd)) and an efficient backtracking algorithm by Kemper et al.^{39,55} The vertical arrow represents the fundamental CH stretch region, while the horizontal band indicates the threshold region of state density (~ 100 sym selected states/cm⁻¹) suggested from high-resolution studies to be necessary for promoting IVR coupling between "bright" and "dark" zeroth order levels. ^{33,35,49,50,54,61,68} Color/shape coding for the calculations: single ring: phenyl (green circles), benzene (red triangles), pyrazine (purple hexagons), pyridazine (gray diamonds), pyridine (dk red squares), naphthalene (red hexagons), phenanthrene (cyan diamonds), anthracene (dk blue squares), pyrene (yellow circles). Note that all the single ring species are well below this critical state density at ~3000 cm⁻¹, which suggests the feasibility of high-resolution infrared detection for any of the corresponding single ring aromatic radical species under supersonically cooled conditions.

summarizes vibrational state density predictions $(\rho(E_{vib}))$ as a function of internal energy for a series of single, double and larger aromatic ring systems, based on simple harmonic frequency predictions (B3LYP/6-311++g(3df,3pd)) and the Kemper backtracking algorithm. 39,55 Given that the arguments here rely on only approximate vibrational state densities, the choice of density functional theory predictions for these frequencies should be entirely adequate. For each of the single aromatic ring species, the density of states at fundamental CH stretch energies is roughly $\rho(E_{\rm vib}) \sim 0.1 {\rm \ states/cm^{-1}}$, with the corresponding numbers of $\rho(E_{\rm vib}) \sim 20 {\rm \ states/cm^{-1}}$ and $\rho(E_{\rm vib})$ ~1000 states/cm⁻¹for double (naphthalene) and triple (phenenthrene, anthracene) aromatic ring systems. Also indicated on this plot is the $\sim 10^2$ states/cm⁻¹ threshold density of states empirically obtained from high-resolution studies for CH stretch excitation in the terminal acetylenes.^{60,61} The predictions for the larger ring systems suggest that spectral congestion due to IVR coupling will be dominant, although results for double aromatic ring systems such as naphthalene may be sufficiently sparse to tackle with high-resolution methods. However, it is also worth noting that these state densities represent extremely rapidly growing functions of internal vibrational energy, and thus any such IVR imposed limits on molecular size in the CH stretch region could be considerably reduced for excitation at lower frequencies. In any event, the data for each of the single aromatic ring systems at the fundamental CH stretch excitation are already consistently 2-3 orders of magnitude below this threshold state density, which clearly bodes well for further study of the corresponding radical species via high resolution IR spectroscopy.

V. SUMMARY AND CONCLUSIONS

The phenyl radical has been studied with high-resolution infrared spectroscopy enabling the identification of the $\nu = 1 \leftarrow$ 0 excitation of the C-H symmetric out-of-phase vibration, ν_{19} . This assignment has been unambiguously confirmed via ground state combination difference band comparison with previously published microwave data,³² with a vibrational band origin determined to high precision ($\nu_0 = 3071.8915(4) \text{ cm}^{-1}$) and over 100 spectrally resolved transitions fit to near experimental uncertainty levels ($\sigma = 11 \text{ MHz} \approx 0.0004 \text{ cm}^{-1}$). The band origin is in quite good agreement with matrix isolation studies $(\nu_{19} = 3072 \text{ cm}^{-1})$ performed by Ellison and co-workers. This would be consistent with a red shift that is remarkably small (\approx 0.96 cm⁻¹) and more typical of those observed under the more weakly perturbative conditions of rare gas Ne matrices or even van der Waals complexes. 30,62-67 Given the relatively large number of atoms and normal modes in phenyl radical, the observed IR spectrum is surprisingly clean and lacks any additional structure and/or broadening due to IVR. Experimental and theoretical analysis of ground and excited state rotational constants help inform on changes in intramolecular bonding due to the half-filled σ molecular orbital, with increased CCC bond angle and decreased bond CC lengths consistent with partial sp versus sp² character for the radicalcarbon atom. Analysis of nuclear spin statistical weights and experimental inertial defects confirm the vibrationally averaged planarity of phenyl as well as the ²A₁ symmetry of the electronic ground state. The feasibility of such a spectral analysis constitutes an important step progress toward high resolution infrared spectroscopy of additional aromatic ring hydrocarbon radical systems, which likely play important roles in both combustion and interstellar chemistry.

AUTHOR INFORMATION

Corresponding Author

*Telephone: 303-492-8857; e-mail: djn@jila.colorado.edu.

Notes

The authors declare no competing financial interest.

ACKNOWLEDGMENTS

This work was supported by grants from the Department of Energy (DE-FG02-09ER16021), with initial funds for construction of the slit jet laser spectrometer provided by the National Science Foundation (CHE 1012685, PHY 1125844). We would also like to congratulate Professor Takeshi Oka for his brilliant spectroscopic accomplishments over so many decades, as well as to thank him for his dedication to and unabashed lifelong celebration of the art of high resolution infrared spectroscopy.

REFERENCES

- (1) Woods, P. M.; Millar, T. J.; Zijlstra, A. A. The Synthesis of Benzene in the Proto-Planetary Nebula CRL 618. *Astrophys. J.* **2002**, 574, L167–L170.
- (2) Glassman, I.; Yetter, R. A. Combustion; Academic Press: San Diego, CA, 2008.
- (3) Wang, H.; Frenklach, M. Calculations of Rate Coefficients for the Chemically Activated Reactions of Acetylene with Vinylic and Aromatic Radicals. *J. Phys. Chem.* **1994**, *98*, 11465–11489.
- (4) Marinov, N. M.; Pitz, W. J.; Westbrook, C. K.; Castaldi, M. J.; Senkan, S. M. Modeling of Aromatic and Polycyclic Aromatic Hydrocarbon Formation in Premixed Methane and Ethane Flames. *Combust. Sci. Technol.* **1996**, *116*, 211–287.
- (5) Frenklach, M.; Warnatz, J. Detailed Modeling of PAH Profiles in a Sooting, Low Pressure Acetylene Flame. *Combust. Sci. Technol.* **1987**, *51*, 265–283.
- (6) Yu, T.; Lin, M. C. Kinetics of the $C_6H_5+O_2$ Reaction at Low Temperatures. J. Am. Chem. Soc. 1994, 116, 9571–9576.
- (7) Park, J.; Dyakov, I. V.; Lin, M. C. FTIR and Mass-Spectrometric Measurements of the Rate Constant for the $C_6H_5+H_2$ Reaction. *J. Phys. Chem. A* **1997**, 101, 8839–8843.
- (8) Mebel, A. M.; Lin, M. C.; Yu, T.; Morokuma, K. Theoretical Study of Potential Energy Surface and Thermal Rate Constants for the $C_6H_5 + H_2$ and $C_6H_6 + H$ Reactions. *J. Phys. Chem. A* **1997**, 101, 3189–3196.
- (9) Yu, T.; Lin, M. C. Kinetics of Phenyl Radical Reactions with Selected Cycloalkanes and Carbon Tetrachloride. *J. Phys. Chem.* **1995**, 99, 8599–8603.
- (10) Yu, T.; Lin, M. C. Kinetics of Phenyl Radical Reactions Studied by the Cavity Ringdown Method. *J. Am. Chem. Soc.* **1993**, *115*, 4371–4372.
- (11) Yu, T.; Lin, M. C. Kinetics of the C_6H_5 + NO Association Reaction. J. Phys. Chem. **1994**, 98, 2105–2109.
- (12) Miller, J. A.; Melius, C. F. Kinetic and Thermodynamic Issues in the Formation of Aromatic Compounds in Flames of Aliphatic Fuels. *Combust. Flame* **1992**, *91*, 21–39.
- (13) Logan, C. F.; Chen, P. Ab Initio Calculation of Hydrogen Abstraction Reactions of Phenyl Radical and p-Benzyne. *J. Am. Chem. Soc.* **1996**, *118*, 2113–2114.
- (14) Kaiser, R. I.; Asvany, O.; Lee, Y. T.; Bettinger, H. F.; Schleyer, P. V.; Schaefer, H. F. Crossed Beam Reaction of Phenyl Radicals with Unsaturated Hydrocarbon Molecules. I. Chemical Dynamics of Phenylmethylacetylene ($C_6H_5CCCH_3;X^{-1}A'$): Formation from Reaction of $C_6H_5(X^{-2}A_1)$ with Methylacetylene, $Ch_3CCH(X^{-1}A_1)$. J. Chem. Phys. **2000**, 112, 4994–5001.
- (15) Niu, J. Y.; Hu, J. Y. Formation and Distribution of Heavy Oil and Tar Sands in China. *Mar. Pet. Geol.* 1999, 16, 85–95.
- (16) Strausz, O. P.; Mojelsky, T. W.; Payzant, J. D.; Olah, G. A.; Prakash, G. K. S. Upgrading of Alberta's Heavy Oils by Superacid-Catalyzed Hydrocracking. *Energy Fuels* **1999**, *13*, 558–569.

- (17) Cook, B. R.; Wilkinson, B. B.; Culross, C. C.; Holmes, S. M.; Martinez, L. E. Hydrogen Transfer Induced Cleavage of Biaryl Bonds. *Energy Fuels* **1997**, *11*, 61–75.
- (18) Agafonov, G. L.; Naydenova, I.; Vlasov, P. A.; Warnatz, J. Detailed Kinetic Modeling of Soot Formation in Shock Tube Pyrolysis and Oxidation of Toluene and *n*-Heptane. *Proc. Combust. Inst.* **2007**, *31*, 575–583.
- (19) Morgan, W. A.; Feigelson, E. D.; Wang, H.; Frenklach, M.; New, A. Mechanism for the Formation of Meteoric Kerogen-Like Material. *Science* **1991**, 252, 109–112.
- (20) Cherchneff, I.; Barker, J. R.; Tielens, A. Polycyclic Aromatic Hydrocarbon Formation in Carbon Rich Stellar Envelopes. *Astrophys. J.* **1992**, *401*, 269–287.
- (21) Appel, J.; Bockhorn, H.; Frenklach, M. Kinetic Modeling of Soot Formation with Detailed Chemistry and Physics: Laminar Premixed Flames of C₂ Hydrocarbons. *Combust. Flame* **2000**, *121*, 122–136.
- (22) Frenklach, M.; Feigelson, E. D. Formation of Polycyclic Aromatic Hydrocarbons in Circumstellar Environments. *Astrophys. J.* **1989**, *341*, *372*–*384*.
- (23) Wang, H.; Frenklach, M. A Detailed Kinetic Modeling Study of Aromatics Formation in Laminar Premixed Acetylene and Ethylene Flames. *Combust. Flame* **1997**, *110*, 173–221.
- (24) Parker, D. S. N.; Zhang, F. T.; Kim, Y. S.; Kaiser, R. I.; Landera, A.; Kislov, V. V.; Mebel, A. M.; Tielens, A. Low Temperature Formation of Naphthalene and Its Role in the Synthesis of PAHs (Polycyclic Aromatic Hydrocarbons) in the Interstellar Medium. *Proc. Natl. Acad. Sci. U.S.A.* **2012**, *109*, 53–58.
- (25) Cernicharo, J.; Heras, A. M.; Tielens, A.; Pardo, J. R.; Herpin, F.; Guelin, M.; Waters, L. Infrared Space Observatory's Discovery of C₄H₂, C₆H₂, and Benzene in CRL 618. *Astrophys. J.* **2001**, 546, L123–L126.
- (26) Weaver, S. L. W.; Remijan, A. J.; McMahon, R. J.; McCall, B. J. A Search for Ortho-Benzyne (o- C_6H_4) in CRL 618. Astrophys. J. Lett. **2007**, 671, L153–L156.
- (27) Pilbratt, G. L.; Riedinger, J. R.; Passvogel, T.; Crone, G.; Doyle, D.; Gageur, U.; Heras, A. M.; Jewell, C.; Metcalfe, L.; Ott, S. Herschel Space Observatory an ESA Facility for Far-Infrared and Submillimetre Astronomy. *Astron. Astrophys.* **2010**, *518*, L1.
- (28) Magnelli, B.; Lutz, D.; Santini, P.; Saintonge, A.; Berta, S.; Albrecht, M.; Altieri, B.; Andreani, P.; Aussel, H.; Bertoldi, F. A Herschel View of the Far-Infrared Properties of Submillimetre Galaxies. *Astron. Astrophys.* **2012**, *539*, A155—.
- (29) Harwit, M. The Herschel Mission. In *Astronomy at IR/Sub-mm and the Microwave Backgound*; Wesselius, P. R., Olthof, H., Eds.; Pergamon-Elsevier Science Ltd: Kidlington, U.K., 2004; Vol. 34, pp 568–572.
- (30) Friderichsen, A. V.; Radziszewski, J. G.; Nimlos, M. R.; Winter, P. R.; Dayton, D. C.; David, D. E.; Ellison, G. B. The Infrared Spectrum of the Matrix-Isolated Phenyl Radical. *J. Am. Chem. Soc.* **2001**, *123*, 1977–1988.
- (31) Sharp, E. N.; Roberts, M. A.; Nesbitt, D. J. Rotationally Resolved Infrared Spectroscopy of a Jet-Cooled Phenyl Radical in the Gas Phase. *Phys. Chem. Chem. Phys.* **2008**, *10*, 6592–6596.
- (32) McMahon, R. J.; McCarthy, M. C.; Gottlieb, C. A.; Dudek, J. B.; Stanton, J. F.; Thaddeus, P. The Radio Spectrum of the Phenyl Radical. *Astrophys. J.* **2003**, *590*, L61–L64.
- (33) McIlroy, A.; Nesbitt, D. J. High-Resolution, Slit Jet Infrared Spectroscopy of Hydrocarbons: Quantum State Specific Mode Mixing in CH Stretch Excited Propyne. *J. Chem. Phys.* **1989**, *91*, 104–113.
- (34) Davis, S.; Uy, D.; Nesbitt, D. J. Laser Spectroscopy of Jet-Cooled Ethyl Radical: Infrared Studies in the CH₂ Stretch Manifold. *J. Chem. Phys.* **2000**, *112*, 1823–1834.
- (35) Lehmann, K. K.; Scoles, G.; Pate, B. H. Intramolecular Dynamics from Eigenstate Resolved Infrared Spectra. *Annu. Rev. Phys. Chem.* **1994**, *45*, 241–274.
- (36) Hopkins, J. B.; Powers, D. E.; Smalley, R. E. Vibrational Relaxation in Jet-Cooled Alkyl Benzenes. 1. Absorption Spectra. *J. Chem. Phys.* **1980**, 72, 5039–5048.

- (37) Davis, S.; Farnik, M.; Uy, D.; Nesbitt, D. J. Concentration Modulation Spectroscopy with a Pulsed Slit Supersonic Discharge Expansion Source. *Chem. Phys. Lett.* **2001**, 344, 23–30.
- (38) Dong, F.; Davis, S.; Nesbitt, D. J. Slit Discharge IR Spectroscopy of a Jet-Cooled Cyclopropyl Radical: Structure and Intramolecular Tunneling Dynamics. J. Phys. Chem. A 2006, 110, 3059–3070.
- (39) Frisch, M. J.; Trucks, G. W.; Schlegel, H. B.; Scuseria, G. E.; Robb, M. A.; Cheeseman, J. R.; Zakrzewski, V. G.; J. A. Montgomery, J.; Stratmann, R. E.; Burant, J. C., et al.. *Gaussian 98*, revision A.7; Gaussian, Inc.: Pittsburgh, PA, 1998.
- (40) Pine, A. S. High Resolution Methane ν_3 Band Spectra Using a Stabilized Tunable Difference Frequency Laser System. *J. Opt. Soc. Am.* **1976**, *66*, 97–108.
- (41) Bunker, P. R.; Jensen, P. Molecular Symmetry and Spectroscopy; NRC Research Press: Ottawa, ON, Canada, 2006.
- (42) Oka, T.; Morino, Y. Calculation of Inertial Defect. 1. General Formulation. *J. Mol. Spectrosc.* **1961**, *6*, 472.
- (43) Oka, T. On Negative Inertial Defect. J. Mol. Struct. 1995, 352, 225-233.
- (44) Jagod, M. F.; Oka, T. Inerial Defects of Planar Symmetric Top Molecules. *J. Mol. Spectrosc.* **1990**, *139*, 313–327.
- (45) Pliva, J.; Pine, A. S. Analysis of the 3 μ m Bands of Benzene. *J. Mol. Spectrosc.* **1987**, 126, 82–98.
- (46) Pliva, J.; Pine, A. S. The Spectrum of Benzene in the 3 μ m Region: The ν_{12} Fundamental Band. *J. Mol. Spectrosc.* **1982**, 93, 209–236.
- (47) Langseth, A.; Stoicheff, B. P. High Resolution Raman Spectroscopy of Gases. 6. Rotational Spectrum of Symmetric Benzene-d₃. *Can. J. Phys.* **1956**, *34*, 350–353.
- (48) Werner, H.-J.; Knowles, P. J.; Lindh, R.; Schutz, M.; Celani, P.; Korona, T.; Manby, F. R.; Rauhut, G.; Amos, R. D.; Bernhardsson, A., et al. *Molpro, Version 2002.6, A Package of Ab Initio Programs*; University of Birmingham: Birmingham, UK: 2003 (See Http://Www. Molpro.Net).
- (49) Nesbitt, D. J.; Field, R. W. Vibrational Energy Flow in Highly Excited Molecules: Role of Intramolecular Vibrational Redistribution. *J. Phys. Chem.* **1996**, *100*, 12735–12756.
- (50) McIlroy, A.; Nesbitt, D. J.; Kerstel, E. R. T.; Pate, B. H.; Lehmann, K. K.; Scoles, G. Sub-Doppler Infrared Laser Spectroscopy of Propyne $2\nu_1$ Band: Evidence for Z-Axis Coriolis Dominated Intramolecular State Mixing in the Acetylenic CH Stretch Overtone. *J. Chem. Phys.* **1994**, *100*, 2596–2611.
- (51) Parmenter, C. S.; Stone, B. M. The Methyl Rotor as an Accelerating Functional Group for IVR. *J. Chem. Phys.* **1986**, *84*, 4710–4711.
- (52) Moss, D. B.; Parmenter, C. S. Acceleration of Intramoleular Vibrational Redistribution by Methyl Internal Rotation: A Chemical Timing Study of p-Fluorotoluene and p-Fluorotoluene-d₃. *J. Chem. Phys.* **1993**, *98*, *6897*–*6905*.
- (53) Coveleskie, R. A.; Dolson, D. A.; Parmenter, C. S. A Direct View of Intramolecular Vibrational Redistribution in S₁ Para-Difluorobenzene. *J. Chem. Phys.* **1980**, *72*, 5774–5775.
- (54) Bethardy, G. A.; Wang, X. L.; Perry, D. S. The Role of Molecular Flexibility in Accelerating Intramolecular Vibrational Relaxation. *Can. J. Chem.-Rev. Can. Chim.* **1994**, *72*, 652–659.
- (55) Kemper, M. J. H.; Vandijk, J. M. F.; Buck, H. M. Backtracking Algorithm for Exact Counting of Internal Molecular Energy Levels. *Chem. Phys. Lett.* **1978**, *53*, 121–124.
- (56) Whitten, G. Z.; Rabinovitch, B. S. Accurate and Facile Approximation for Vibrational Energy Level Sums. *J. Chem. Phys.* **1963**, 38, 2466.
- (57) Tardy, D. C.; Rabinovi, Bs; Whitten, G. Z. Vibration-Rotation Energy Level Density Calculations. *J. Chem. Phys.* **1968**, *48*, 1427.
- (58) Callegari, A.; Merker, U.; Engels, P.; Srivastava, H. K.; Lehmann, K. K.; Scoles, G. Intramolecular Vibrational Redistribution in Aromatic Molecules. I. Eigenstate Resolved CH Stretch First Overtone Spectra of Benzene. *J. Chem. Phys.* **2000**, *113*, 10583–10596.

- (59) Hopkins, J. B.; Powers, D. E.; Smalley, R. E. Predissociation Probes of Vibrational Energy Localization. *J. Chem. Phys.* **1981**, *74*, 745–747.
- (60) Mcllroy, A.; Nesbitt, D. J. Large-Amplitude Skeletal Isomerization as a Promoter of Intramolecular Vibrational-Relaxation in CH Stretch Excited Hydrocarbons. *J. Chem. Phys.* **1994**, *101*, 3421–3435.
- (61) McIlroy, A., Nesbitt, D. J. Vibrational-Mode Mixing in Terminal Acetylenes High-Resolution Infrared-Laser Study of Isolated J States. *J. Chem. Phys.* **1990**, *92*, 2229–2243.
- (62) McIlroy, A.; Lascola, R.; Lovejoy, C. M.; Nesbitt, D. J. Structural Dependence of HF Vibrational Red Shifts in Ar_nHF , n=1-4, via High-Resolution Slit Jet Infrared-Spectroscopy. *J. Phys. Chem.* **1991**, 95, 2636–2644.
- (63) Clary, D. C.; Lovejoy, C. M.; ONeil, S. V.; Nesbitt, D. J. Infrared-Spectrum of NeHF. *Phys. Rev. Lett.* **1988**, *61*, 1576–1579.
- (64) Lovejoy, C. M.; Nesbitt, D. J. The Near-Infrared Spectrum of NeHCl. Chem. Phys. Lett. 1988, 147, 490-496.
- (65) Lovejoy, C. M.; Nesbitt, D. J. Mode Specific Internal and Direct Rotational Predissociation in HeHF, HeDF, and HeHCl van der Waals Complexes in the Weak Binding Limit. *J. Chem. Phys.* **1990**, *93*, 5387–5407.
- (66) Lovejoy, C. M.; Nesbitt, D. J. Rotational Predissociation, Vibrational Mixing, and van der Waals Intermolecular Potentials of NeDF. *J. Chem. Phys.* **1991**, *94*, 208–223.
- (67) Jacox, M. E.; Thompson, W. E. The Infrared Spectroscopy and Photochemistry of NO₃ Trapped in Solid Neon. *J. Chem. Phys.* **2008**, 129, 204306.
- (68) Pate, B. H.; Lehmann, K. K.; Scoles, G. The Onset of Intramolecular Vibrational Energy Redistribution and Its Intermediate Case: The ν_1 and $2\nu_1$ Molecular Beam, Optothermal Spectra of Trifluoropropyne. *J. Chem. Phys.* **1991**, *95*, 3891–3916.
- (69) Stoicheff, B. P. High Resolution Raman Scpectroscopy of Gases. 2. Rotational Spectrum of C_6H_6 and C_6D_6 and Internuclear Distances in the Benzene Molecule. *Can. J. Phys.* **1954**, 32, 339–&.